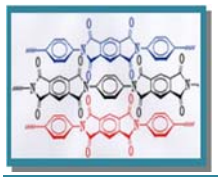

STEPI 9
Polyimides & High Perfomance Polymers
3-5 June 2013
Montpellier, France

Enhanced Thermal Conductivity Based on Vertical Double Percolation Morphology in Phase Separated Polyimide Blend Films Containing Silver or Metal Oxide Particles

Shinji ANDO*, Tomoya MURAKAMI, and Daisuke YORIFUJI

Dept. Chemistry and Materials Science, Tokyo Institute of Technology,
Ookayama 2-12-1-E4-5, Meguro-ku, Tokyo 152-8552, Japan
Tel : +81-3-5734-2137, Fax : +81-3-5734-2889, E-mail : sando@polymer.titech.ac.jp

1. Introduction

Heat generation and exothermic density of electric and electronic devices are tremendously increasing with high speed and high integration of latest semiconductor devices. Thereby, it is strongly required to enhance the thermal conductivity of polymeric heat dissipation materials used for adhesion between metallic and semi-conductor devices and substrates in power-electronics and automobile-electronics applications.

Polyimide (PI) is a representative super engineering plastic which exhibit outstanding mechanical strength, heat resistance, good processability, and electric insulating properties. PIs have been widely used as insulating films and surface protection (buffer coat) films in semiconductor industries. Although improvement in thermally conductivity is strongly expected, polymers are inherently dielectric materials, and their thermal conductivity (0.1–0.5 W/m·K) is much lower than those of metals and ceramics. From a viewpoint of heat transfer of substance via thermal vibration, average mean free path of acoustic phonon is isotropic in amorphous or semi-crystalline polymers like PIs. However, large anisotropy in thermal conductivity is observed for uniaxially oriented polymer films [1–3] because average phonon velocity is highly anisotropic in the directions between parallel and perpendicular to the polymer chains.

Composite materials consisting of polymer matrix and inorganic (metals or ceramics) fillers exhibiting high thermal conductivity has been widely developed for many years, however it is still difficult to attain high thermal conductivity only by homogeneous dispersion of fillers in polymer matrices. Moreover, high filler content generally causes serious deterioration of physical properties such as mechanical strength and toughness, adhesiveness, processability, insulation properties, surface flatness, etc. Thereby, we have been pursuing new materials design concepts which enables to surpass the thermal conductivity attainable by conventional technology with much lower filler contents.

The former part of this article describe the relationships among the thermal conductivity of PI films in the thickness direction, the molecular structure, and the states of molecular packing of PI films. When PIs are applied to heat dissipation sheet and interlayer insulation films, the thermal conductivity in the thickness direction is of special importance. In the latter part, a novel technique to prepare PI blend films with vertical phase separation morphology, which exhibit enhanced thermal conductivity, using thermally conductive fillers, such as silver (Ag) nanoparticles, zinc oxide (ZnO), and magnesium oxide (MgO) particles, is explained.

2. Analysis of Thermal diffusivity of PI films

2.1 Relations between molecular structure, in-plane orientation, molecular packing, and out-of-plane thermal diffusivity[6]

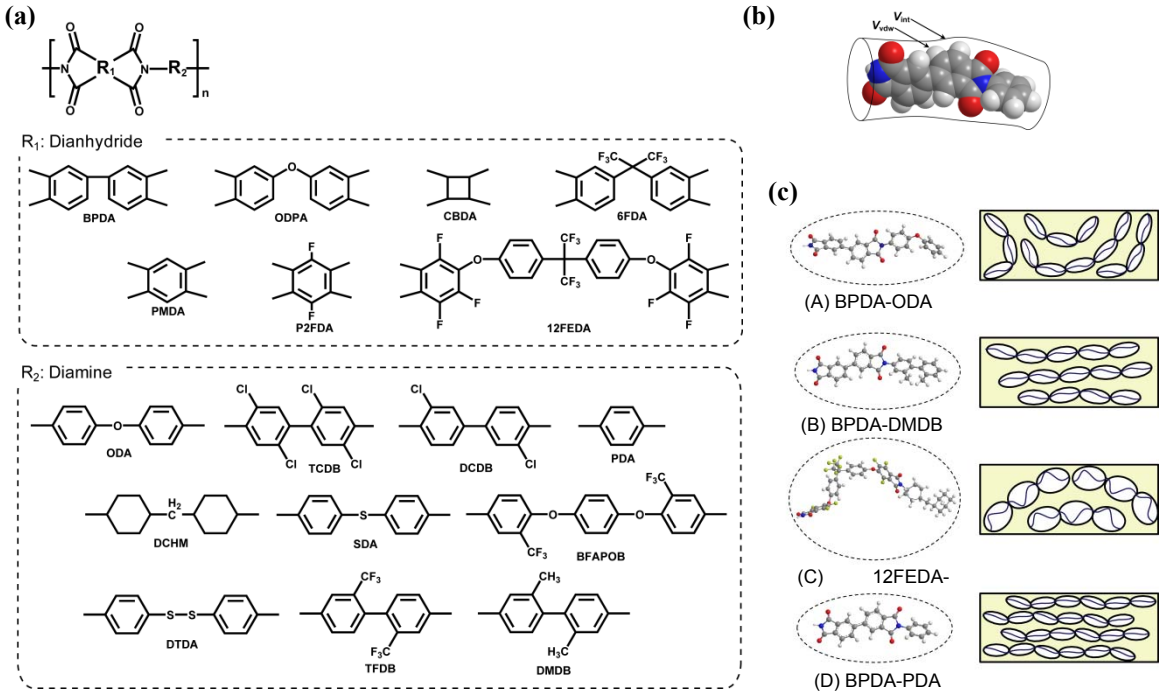

Fig. 1 (a) Structures of PIs, (b) Schematic figures of V_{int} and V_{vdw}, (c) Optimized structures of PI repeating units (left) and cross-sectional views of molecular orientation and packing states in PI films (right).

As shown in Fig. 1(a), 21 kinds of PI films (thickness: 15-39 μm) were prepared using 7 kinds of tetracarboxylic acid dianhydrides and 10 kinds of diamines by the conventional two-step method using poly(amic acid)s (PAAs) as precursors. The final curing temperature was 350°C. Thermal diffusivity in the thickness direction ($D_\perp$) of PI films was measured by AC temperature wave analysis (TWA)[4–5] with *ai*-Phase Mobile-1u. The $D_\perp$ values of PIs are in the range of 8.9–18.3 x 10^{-8} m^2/s, in which the largest $D_\perp$ of *s*BPDA-ODA is twice larger than the smallest of 12FEFA-DCHM. The out-of-plane thermal conductivity ($a_\perp$) estimated using the measured $D_\perp$, standard density and heat capacity are 0.14–0.28 W/m·K.[6] During spin-coating process for film forming, PAA chains are oriented in the in-plane direction by circumferential stress due to centrifugal force. The degrees of in-plane orientation of PI chains are significantly dependent on the rigidity/linearity of repeating unit.

The molecular structure and the higher order structure of PI film were evaluated based on the following three factors; (1) the degree of main chain orientation, (2) the rigidity/linearity of molecular structure, and (3) the aggregation structure and state of molecular packing of polymer chains. We have tried quantitative estimation of these factors by using (1) experimental in-plane/out-of-plane birefringence (Δn), (2) polarizability anisotropy of PI chains estimated by quantum chemical calculations (density functional theory, DFT), and (3) molecular packing coefficient (K_p) estimated from experimental average refractive indices and calculated molecular polarizability. In-plane ($n_{//}$) and out-of-plane refractive indices ($n_\perp$) were measured by a prism coupler (Metricon PC-2010) at the wavelength of 1324 nm. Average refractive index (n_{av}) and Δn were calculated by the following equations.

$$\Delta n = n_{//} - n_\perp \qquad (1)$$

$$n_{av} = \frac{2n_{//} + n_\perp}{3} \qquad (2)$$

Principal values of molecular polarizability tensor (α_{XX}, α_{YY}, α_{ZZ}) were calculated by DFT using the B3LYP functional and 6-311++G(d,p) basis set. Molecular geometries of model compounds were optimized using the 6-311G(d) basis set prior to polarizability calculations. The tensor component of α_{XX} is

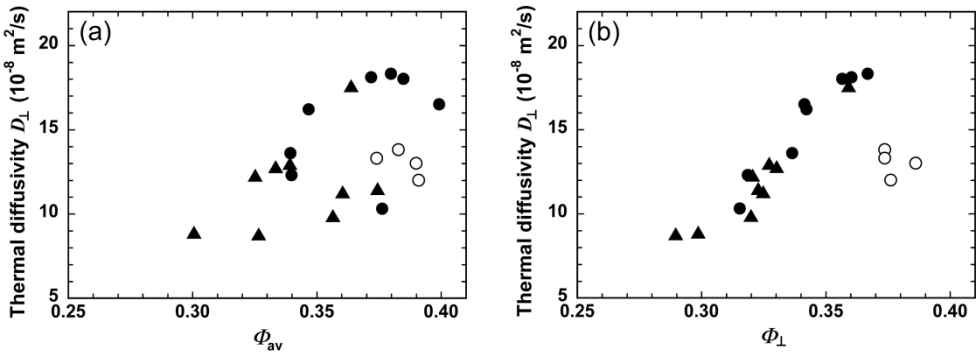

Fig. 2 Relationships between $D_\perp$ and Lorentz parameter Φ_{av} (left), and that between $D_\perp$ and Vuks parameter $\Phi_\perp$ (right). Sulfur-containing PIs are depicted by open symbols due to their inherently low $D_\perp$.

pointing parallel to 5-membered imide ring, α_{YY} is perpendicular to imide ring, and α_{ZZ} is parallel to the PI main chain. Average polarizability (α_{av}) and anisotropy in polarizability tensor ($\Delta\alpha$) were calculated by the following equations.

$$\Delta\alpha = \alpha_{ZZ} - \frac{\alpha_{XX} + \alpha_{YY}}{2} \quad (3)$$

$$\alpha_{av} = \frac{\alpha_{XX} + \alpha_{YY} + \alpha_{ZZ}}{3} \quad (4)$$

Moreover, van der Waals volumes (V_{vdw}) of PIs were calculated according to the Slonimskii's method[7] using geometries optimized by DFT and van der Waals radii of atoms reported by Bondi.[8] On the other hand, packing coefficient, K_p, which represents the aggregation state of polymer chains is defined as follows.[9]

$$K_p = \frac{V_{vdw}}{V_{int}} \quad (5)$$

where V_{int} is molecular volume, which is a sum of intermolecular free volume and V_{vdw}. The values of K_p were calculated from experimental n_{av} and calculated α_{av}/V_{vdw} using the formula previously proposed by us[9] :

$$\Phi_{av} \equiv \frac{n_{av}^2 - 1}{n_{av}^2 + 2} = \frac{4\pi}{3}\frac{K_p}{V_{vdw}}\alpha_{av} \quad (6)$$

Four kinds of PIs having characteristic molecular and aggregation structures are shown in Fig. 1(c) as typical examples. When $\Delta\alpha/V_{vdw}$ of a PI is large with a rigid/linear structure, the ellipse (dotted line) surrounding the repeating units (left-hand side) becomes more elongated. In the cross-sectional schemes of films (right-hand side), PI chains are expressed by connected ellipses representing polarizability anisotropy. The orientation of PI chains becomes isotropic, when Δn is small. Considering the relationship between the experimental $D_\perp$ and molecular structures, PIs like BPDA-ODA (A) consisting of a rigid/linear BPDA component and a bent and rotatable ODA component exhibited the largest $D_\perp$ (18.3 x 10^{-8} m_2/s). On the other hand, PIs like BPDA-DMDB (B) consisting of linear structure with bulky side chains (−CH_3), and PIs like 12FEDA-DCHM (C) including plural bent and rotatable linkages with highly flexible structures exhibited much smaller $D_\perp$ values.

These facts indicate that key-points for high thermal diffusivity are as follows: (1) wholly linear structure of polymer chain which increase the mean-free-path of phonon, (2) inclusion of one bent (−O−) structure which reduce the total in-plane orientation of PI chains, and (3) absence of bulky side chains. A classical idea that thermal energy is principally transmitted through covalently-bonded main chains with atomic vibrations looks appropriate in case of several tens of μm-thick PI films as well. Moreover, although the PI chains are highly oriented in the film plane as same as (B), BPDA-PDA (D) with a large K_p value, which indicates densely packed polymer chains, exhibited a large $D_\perp$ (16.5 x 10^{-8} m^2/s). Although the dominant factor for $D_\perp$ is orientation of PI chains, the aggregation structure and states of molecular packing is another essential factor.

2.2 Prediction theory for thermal diffusivity of PI films in the out-of-plane direction

As shown in Fig. 2(a). the Φ_{av} values of PIs

reveal a weak and positive correlation with $D_\perp$, but the relationship is unclear. This is because the parameter Φ_{av} only reflects the isotropic properties (average polarizability and molecular packing) without including factors for PI chain orientation as represented by Δn, nonetheless $D_\perp$ is an anisotropic property. Thus, based on the Vuks equation[10] which correlates the polarizability anisotropy of polymers with the anisotropic refraction of light, we defined a new parameter, $\Phi_\perp$ designated as "Vuks parameter", as follows:

$$\Phi_\perp \equiv \frac{n_\perp^{\,2}-1}{n_{av}^{\,2}+2} = \frac{4\pi}{3} K_p \frac{\overline{\alpha}_\perp}{V_{vdw}} \quad (7)$$

As compared with Φ_{av} of eq. (6), $\Phi_\perp$ has a feature in which n_{av} is replaced by out-of-plane refractive index ($n_\perp$). The term, $\alpha_\perp/V_{vdw}$, is the macroscopic out-of-plane polarizability of PI chains per unit volume. Thus, a PI film with a large fraction of out-of-plane oriented main chains (e.g., BPDA-ODA) exhibits a large $\alpha_\perp$ value. The relationship between $D_\perp$ and $\Phi_\perp$ is plotted in Fig. 2(b). Note that the $\Phi_\perp$ values revealed an apparent positive correlation with $D_\perp$ except for the PIs including sulfur atoms in the main chain. These sulfur-containing PIs showed significantly smaller $D_\perp$ values than those expected from their $\Phi_\perp$. This phenomenon is explainable by the reduced average phonon velocity along the polymer chains due to the heavy atom effect.[11] For the PIs derived from BPDA dianhydride, the $\Phi_\perp$ values decreased in the order of diamine moieties: DTDA > SDA > ODA > TCDB > DCDB > PDA > DCHM > BFAPOB > TFDB > DMDB. This order is nearly the same as that of $D_\perp$ values except for the sulfur-containing PIs. On the other hand, the PIs derived from ODA diamine exhibited $\Phi_\perp$ values in the order of dianhydride moieties: BPDA > ODPA > CBDA > P2FDA > PMDA > 6FDA. This order is also nearly the same as that of $D_\perp$ when compared with that of Φ_{av} values. As a result, it was clarified that large $D_\perp$ values were observed for the PIs which demonstrate (1) nearly isotropic main chain orientation in the films, (2) rigid and linear chemical structures without bulky side chains, and (3) dense molecular packing. The Vuks parameter $\Phi_\perp$ can be used as a key measure for predicting the thermal conductivity of amorphous polymers.[6]

3. Enhancement of Thermal Conductivity of PI/Inorganic Hybrid Films

This part introduces three kinds of materials systems which enhance the out-of-plane thermal conductivity of PI films by "hybridization of PIs" with thermally conductive metal (Ag) and ceramic (ZnO, MgO) particles.

3.1 PI blend/Ag nanoparticle Hybrid film

In conventional inorganic/polymer hybrid materials in which μm-size inorganic particles (generally, metal oxide) are dispersed in polymer matrices in the molten state, high filler contents are required for generating heat conducting pathways through sequential contact of particles as predicted by Maxwell[11] and Bruggemen[12]. In general, when critical percolation concentration for enhanced heat conduction is achieved, light weight, flexibility, adhesiveness, and processability of hybrid films are lost. Moreover, when nm-size particles are uniformly dispersed in a polymer matrix, sufficient thermal conductivity is hardly achieved due to interfacial thermal resistance resulting from increased specific surface area of particles and enhanced interactions between particles and matrix. Thereby, aiming at effective enhancement of $D_\perp$ of PI hybrid films, we tried to precipitate silver-nanoparticle in immiscible PI blends consisting of two kinds of PIs with different polarities via *'in-situ* precipitation method'.[13,14] When 'vertical phase separation structure' is formed, in which silver nano-particles (Ag-NP) are selectively incorporated in one phase and excluded from another phase, along the film thickness direction, the former phase should function as an effective thermal conduction pathway.

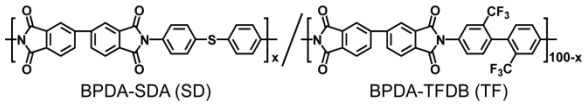

Scheme 1. PIs generating VDP phase separation.

We have prepared mixture solution of silver nitrate ($AgNO_3$) and precursors (PAAs) of a sulfur-containing (BPDA-SDA(SD)) and

fluorine-containing PIs (BPDA-TFDB(TF)), followed by spin-coating and thermal curing at 350°C (Scheme 1). Since these PIs are immiscible to each other, and Ag^+ ions are selectively included in the SD phase, distinct phase-separation morphology was observed for 15–35 μm thick films, when the molar ratio was set to SD : TF : Ag = 70 : 30 : 20 (Fig. 3(a)).

From the cross-sectional SEM micrograph of PI blend film (Fig. 3(b)), 'vertical double percolation (VDP)' morphology is observed, in

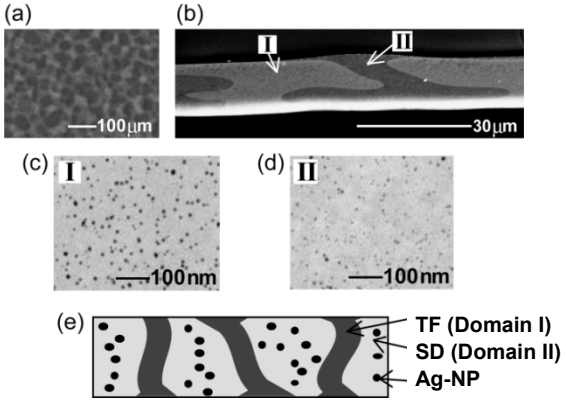

Fig. 3 Phase separation and selective incorporation of Ag-NPs in PI blend films (SD:TF:$AgNO_3$=70:30: 20 mol%) (a) Surface view by optical microscope (50 x), (b) Cross-sectional SEM micrograph, (c) Cross-sectional TEM micrographs of Domain I, and (d) II, (e) Schematic VDP morphology containing Ag-NP.

which the two phases are well separated at 30~50 μm order, and each phase penetrates the film in the thickness direction.[15] Based on microscopic FT-IR spectra, Domain 'I' and 'II' correspond to SD-rich phase and TF-rich phase, respectively. Moreover, based on the TEM micrograph (Figs. 3(c–d)) and X-ray diffraction patterns, it was clarified that crystalline Ag-NP (diameter: 10–30 nm) are preferentially precipitated in the SD phase. Fig. 3(e) shows a schematic figure of VDP morphology thus formed. Due to the strong affinity of Ag^+ to sulfur in SD phase, Ag^+ ions were spontaneously incorporated in SD phase and thermally reduced and precipitated as Ag-NP during imidization. Furthermore, the $D_\perp$ values observed for PI blend films with VDP morphology were significantly larger than those of mono-phase PIs (SD or TF) containing the same amount of Ag-NP[15]. Fig. 4 shows the variations of $D_\perp$ and cross-sectional SEM micrographs of PI blend films with different SD content ($AgNO_3$ content was fixed to 0.5 vol%) In case of (C, SD:TF=50:50), displaying distinct VDF morphology, shows a larger $D_\perp$ (19.4×10^{-8} m^2/s) than those of (A) 30:70 and (B) 60:40. This fact indicated that SD phase containing a large amount of Ag-NP functions as an effective thermal conduction pathway along the thickness direction. The formation of VDP morphology and selective concentration of Ag-NP is effective to produce a novel PI hybrid material with higher thermal conductivity at lower filler content.

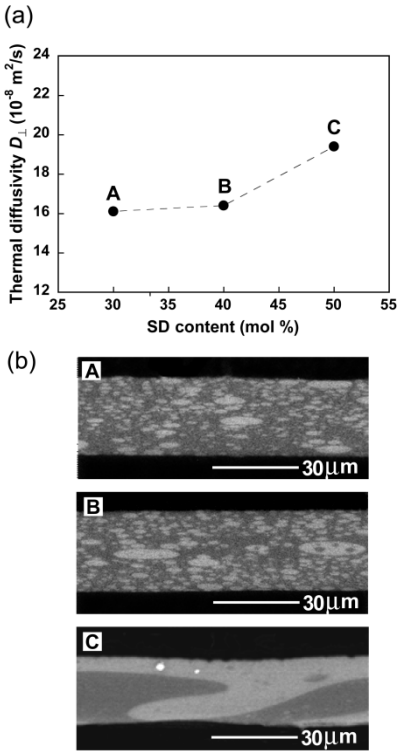

Fig. 4 SD content dependence of (a) $D_\perp$ and (b) cross-sectional SEMs for PI blend films containing Ag-NP. Distinct 'VDP morphology' is seen in (C).

3.2 PI blend/ZnO Nanoparticle Hybrid film

For further enhancement of $D_\perp$ in SD/TF PI blend films with VDP morphology, ZnO nanoparticles were chosen as a new filler. Although Ag-NP shows good thermal conductivity, its high electrical conductivity deteriorates the insulation properties of hybrids. Moreover, inorganic fillers with very small size become a drawback for reducing interfacial thermal resistance at filler surface.[16,17] Since crystalline ZnO shows a high thermal conductivity of 56 W/m·K, we prepared six-sided nano-pyramidal ZnO particles with ~300 nm diameter (ZnO-N, Fig. 5) by refluxing zinc acetate dihydrate $Zn(CH_3COO)\cdot 2H_2O$ in an

oleylamine solution at 240°C for 40 min. The precipitates were separated by centrifuge, washed with ethanol, and then dried under vacuum at room temperature. ZnO-NP was mixed with SD/TF PAA blend solutions to give ZnO-hybridized PI films. The SD:TF ratio was set to 50:50, and the ZnO-NP content was raised up to 27 vol%.[18] The height and base length of ZnO-NP were ca. 500 nm (Fig. 5). The formation of crystalline ZnO was confirmed by wide-angle X-ray diffraction.

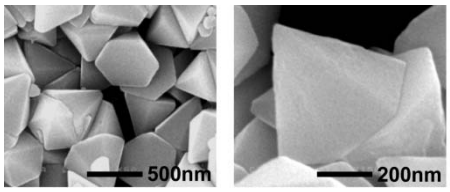

Fig. 5 SEM micrographs of six-sided nano-pyramidal ZnO particles.

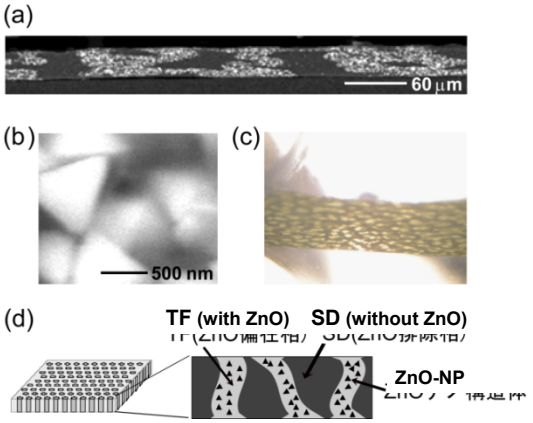

Fig. 6 Phase separation and selective incorporation of ZnO-NP in PI blend films (ZnO:10 vol%). (a) Cross-sectional SEM image, (b) ZnO particles included in TF phase, (c) Surface view by optical microscope (50x), and (d) Schematic view of VDP morphology with selectively incorporated ZnO-NP.

As shown in Fig. 6, distinct VDP morphology was observed in the cross-section of PI blend film. In addition, the TEM micrograph and microscopic FT-IR spectra indicated that ZnO-NPs are preferentially incorporated in TF phase, which is opposite from the case of Ag-NP precipitating in the SD phase. Fig. 6(d) shows a schematic VDP morphology with ZnO-NP.

Fig. 7(a) shows the relationships between $D_{\perp}$ and ZnO content for PI blend films (●, ▲) and mono-phase TF film (■) in which ZnO-NPs are homogeneously dispersed. Fig. 7(b) shows the SEM micrographs of PI blend films which correspond to 'A–I' in Fig. 7(a). The $D_{\perp}$ values observed for distinct VDP morphology (A–C) are significantly larger than those of disordered VDP phase (D–F) and homogeneously dispersed homo-PI (G–I). The effectiveness and advantage of VDP formation is well confirmed.

The out-of-plane thermal conductivities ($a_{\perp}$) were calculated by using the experimental $D_{\perp}$ values, density, and specific heat capacity for the PI blend films forming VDP morphology. They are plotted as '●' in Fig. 8(a). The $a_{\perp}$ values estimated based on the Bruggeman's theory[12] by assuming perfect cylinder-shape phase separation, in which ZnO-NPs are selectively incorporated in the TF phase, is expressed by solid line.[18] For comparison, the experimental $a_{\perp}$ values of homogeneously dispersed TF phase are shown by '■' with calculated values based on the Bruggeman's theory (dashed line). It is obvious that the $a_{\perp}$ values observed with distinct VDP morphology prepared under optimized conditions are much larger than those of homogeneously dispersed PI films; the largest $a_{\perp}$ of 1.54 W/m·K was obtained at a ZnO content

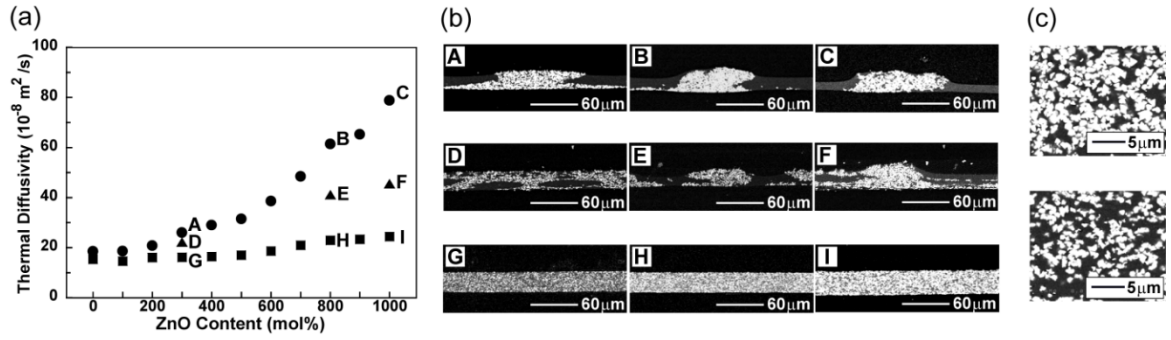

Fig. 7 (a) ZnO content dependence of $D_{\perp}$ values observed for PI blend films containing ZnO-NP, (b) Cross-sectional SEM micrographs of blend films corresponding to A–I in (a), and (c) Magnified views of ZnO-concentrated phase with VDP ('B', top) and homogeneously dispersed phase ('H', bottom).

of 27 vol%, which is 5.1 times larger than that of PI blend film without ZnO-NP. Moreover, the calculated $a_\perp$ values (solid and dashed lines) agree well with the experimental values, which indicates that ideal VDP morphology with densely confined ZnO-NP in the TF phase was formed in the PI blend films. In addition, good film flexibility and high thermal stability with a 5% degradation temp (T_d^5) over 500°C reveals that this material is suitable for thermal interface materials for future electronic applications.

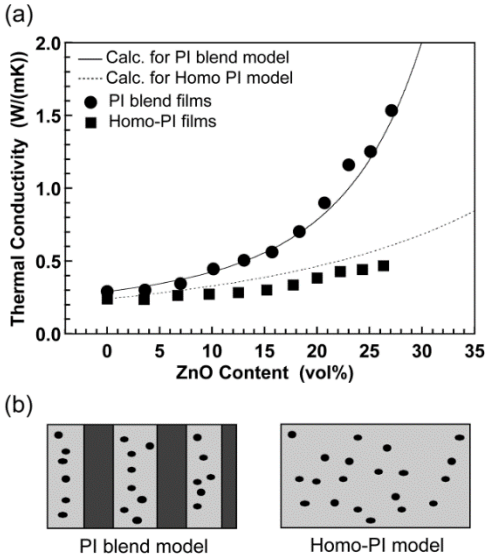

Fig. 8 (a) ZnO content dependence of experimental (● and ■) and calculated (solid and dashed lines) thermal conductivities ($a_\perp$) of PI blend films, (b) Schematic views for ideal model structures for PI blends with VDP structures (left) and for homo-PIs with homogeneously dispersed ZnO-NPs (right).

3.3 PI blend/MgO Microparticle Hybrid film

For further enhancement of $D_\perp$ in PI blend films with VDP morphology, MgO micro-size particles (average diameter : 2.0 μm, Ube materials Industry, Fig. 9) were chosen as new filler for SD/TF PI blends, and the effects of filler size on $D_\perp$ values were investigated.[20] MgO particles showed high crystallinity, and the thermal conductivity of crystalline MgO is 54 W/m·K which is very close to that of ZnO.

The observed $D_\perp$ values for the PI blend films and homo-TF films containing MgO particles are plotted against the MgO content in Fig. 10(a). All the PI blend films in which MgO particles are selectively incorporated in one phase (●, ■, ▲, and ◢) shows larger $D_\perp$ values than the mono-phase TF-PI films with homogeneously dispersed MgO (◆) over a whole range of MgO content (0–29.8 vol%).[20] Moreover, the $D_\perp$ values observed for the PI blend films with clear phase separation (●, ■), which exhibit distinct VDP morphology, showed significantly larger $D_\perp$ than those with deformed phase separation (▲, ◢), in which the phase separated domains do not show vertical penetration structure.[21] The schematic figures and the SEM micrographs for the former and the latter cases are shown in Fig. 10(b)–(e).

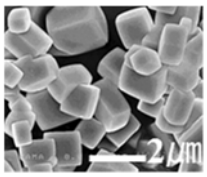

Fig. 9 SEM micrograph of MgO micro-particles

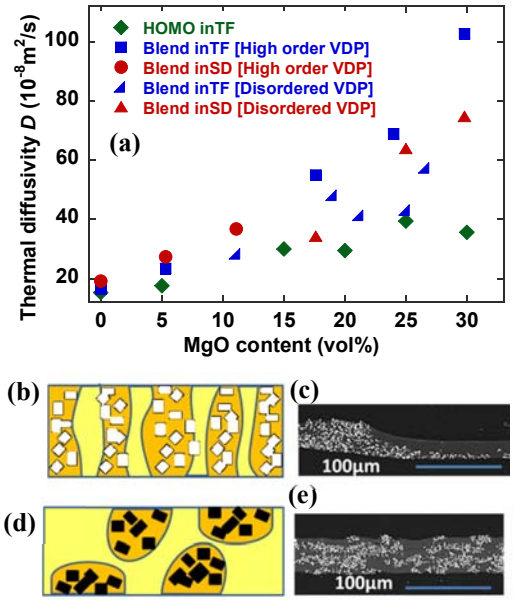

Fig. 10 (a) MgO content dependence of experimental thermal conductivities ($a_\perp$) of PI blend films. Symbols ●, ■ denote distinct VDP morphology, ▲ and ◢ denote disordered VDP morphology, and ◆ denote homogeneously dispersed TF-PI films. (b) and (d) show schematic pictures for distinct and disordered VDP morphology with the corresponding SEM micrographs of (c) and (d), respectively.

A similar phenomena were already observed for the ZnO-NP dispersed PI blend films. Since the thermal conductivity of MgO crystallites is almost the same as that of ZnO, influence of filler size (i.e. filler size effect) can be elucidated without effects of filler species. When the $D_\perp$ of

TF-PI hybrids are compared at the same filler content, MgO-dispersed films entirely exhibit larger $D_{\perp}$ values than ZnO-dispersed films, which indicates that large filler size endow higher thermal diffusivity to the hybrids due to the reduction of thermal flux passing through the hetero-interfaces having high thermal resistance between filler and polymer. In particular, because the PI hybrid films are ca. 30 μm-thick, the influence of increase in filler diameter from 0.5 μm (ZnO) to 2 μm (MgO) is significant. When PI blend films exhibiting distinct VDP

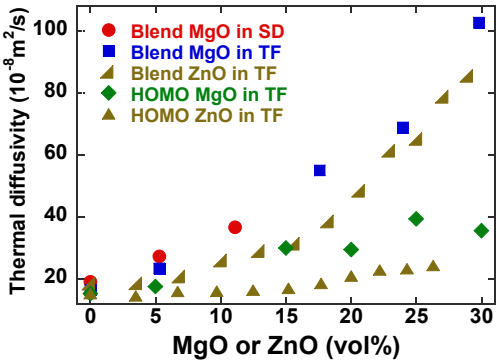

Fig. 11 Filler content dependence of experimental $D_{\perp}$ values of PI blend films containing ZnO-NP and MgO particles. ●,■ : MgO-dispersed PI blends, ◢ : ZnO-dispersed PI blends, ◆ : MgO-dispersed TF-PI, ▲ : ZnO-dispersed TF-PI.

morphology are compared with mono-phase TF-PI films with homogenous filler dispersion, ZnO-dispersed PI blends display large increase in $D_{\perp}$ compared with TF-PI even below 15 vol%, and the increasing trend of $D_{\perp}$ becomes significant over 15 vol%. The $D_{\perp}$ values reach several times larger than those of TF-PI films. Over the filler content at which $D_{\perp}$ shows rapid increase, what we call 'percolation threshold', thermal energy is efficiently transferred via acoustic phonons through well-developed network of physically connected particles.

In the case of MgO-dispersed PI blend films exhibiting distinct VDP morphology, nearly constant increase in $D_{\perp}$ was observed between 0 and 29.8 vol% of MgO content, which is different from the trend in the ZnO-dispersed PI blends. No clear percolation threshold was observed in the MgO case, and the increase in $D_{\perp}$ is significant even at lower filler contents. These facts are attributable to the large size of MgO particles which facilitate mutual physical contact among particles. In contrast, ZnO-dispersed PI blend films surpass the percolation threshold at around 15 vol%, and then their $D_{\perp}$ showed significant increase over the content. Their $D_{\perp}$ values became close to those of MgO-dispersed PI blend films over 25 vol% because of the formation of developed percolation network among ZnO-NPs. These facts indicates that the filler size effect, *i.e.* the advantage of large filler size of MgO, is significant at relatively lower filler content (5–25 vol%), and it became less effective at higher filler content.

4. Conclusion

The relationships between the molecular and higher-order structures and the out-of-plane thermal diffusivity ($D_{\perp}$) of PI films are extensively investigated based on (1) the degree of main chain orientation, (2) the rigidity/linearity of molecular structure, and (3) the aggregation structure and state of molecular packing of PI chains. In addition, the usefulness and effectiveness of the Vuks parameter ($\Phi_{\perp}$) for predicting the $D_{\perp}$ of PIs are examined and confirmed. Furthermore, three kinds of material systems, which significantly enhance the thermal conductivity of PI films in the thickness direction by "hybridization of PIs" with thermally conductive metal (Ag) and ceramic (ZnO, MgO) particles, were demonstrated. In particular, PI blend films composed of a sulfur- and a fluorine-containing PI were prepared via spin-coating and thermal curing of PAA solutions containing ZnO and MgO particles. Microphase-separated structures with "vertical double percolation (VDP)" morphology were spontaneously formed in the films, in which two phases were separately aligned along the out-of-plane direction, and particles were incorporated in one PI phase. The blend films exhibited significant enhancement of thermal conductivity compared with the mono-phase TF-PI films containing homogeneously dispersed particles. These results indicate that the VDP structure with selective incorporation of thermally conductive fillers functions as a very effective thermal conductive pathway.

Acknowledgement

The authors thank Prof. T. Hashimoto and Prof. J. Morikawa of Tokyo Institute of Technology for helpful advice on thermal diffusivity measurements. We would also like to acknowledge Mr. Jun Kouki (Center for Advanced Materials Analysis, Tokyo Institute of Technology) for preparation of cross-section samples and for his valuable suggestions and support. A part of this work was supported by New Energy and Industrial Technology Organization (NEDO). The WAXD experiments were performed with a BL40B2 beamline with the approval of the Japan Synchrotron Radiation Research Institute (JASRI) (Proposal No. 2010A-1090, 2011A-1237]).

Reference

1) C. L. Choy, *Polymer*, **18**, 984 (1977).
2) K. Kurabayashi, *Int. J. Thermophys.*, **22**, 277 (2001).
3) K. Kurabayashi and K. E. Goodson, *J. Appl. Phys.*, **86**, 1925 (1999).
4) J. Morikawa and T. Hashimoto, *Therm. Acta.*, **304**/**305**, 151 (1997).
5) J. Morikawa, J. Tan, and T. Hashimoto, *Polymer*, **36**, 4439 (1995).
6) D. Yorifuji and S. Ando, *Macromolecules*, **43**, 7583 (2010).
7) G. Slonimskii, *Polym. Sci. USSR*, **12**, 556 (2010).
8) A. Bondi, *J. Phys. Chem.*, **68**, 441 (1964).
9) Y. Terui and S. Ando., *J. Polym. Sci. B*, **42**, 2354 (2004).
10) M. F. Vuks, *Opt. Spectrosc.*, **20**, 361 (1964).
11) J. C. Maxwell, "*Electricity and Magnetism*" Clarendon Press, Oxford, UK (1873).
12) D. A. G. Bruggeman, *Ann. Phys.*, **24**, 645 (1936).
13) T. Sawada and S. Ando, *Chem. Mater.*, **10**, 3368 (1998).
14) K. Murakami and S. Ando, *J. Photopolym. Sci. Technol.*, **23**, 501 (2010).
15) D. Yorifuji and S. Ando, *Macromol. Chem. Phys.*, **211**, 2118 (2010).
16) W. Zhou, S. Qi, C. Tu, H. Zhao, C. Wang, and J. Kou, *J. Appl. Polym. Sci.*, **104**, 1312 (2007).
17) A. Devpura, P. E. Phelan, and R. S. Prasher, *Micro. Thermophys. Eng.*, **5**, 177 (2001).
18) D. Yorifuji, and S. Ando, *J. Mater. Chem.*, **21**, 4402 (2011).
19) D. Yorifuji, and S. Ando, *Polym. Prep. Jpn.*, **59**, 969 (2009).
20) T. Murakami and S. Ando, *Proc. Thermophys. Prop. Conf. Jpn.*, **32**, 308 (2012).
21) T. Murakami and S. Ando, *Polym. Prep. Jpn.*, **61**, 4711 (2012).